Materials Science and Technology 31 (2015) 1066-1076

The austenite–ferrite transformation in enhanced-niobium, low-carbon steel

P. Yan*, H. K. D. H. Bhadeshia

Materials Science and Metallurgy, University of Cambridge

Abstract

The austenite to ferrite transformation characteristics of a commercial high strength line pipe steel containing 0.05 wt% carbon and 0.095 wt% niobium have been rigorously studied by continuous cooling experiments in the 960°C to 1260°C range. A remarkable delay in the austenite to allotriomorphic ferrite transformation has been demonstrated to occur under practically relevant thermal processing conditions. The effects of prior austenite grain size and soluble niobium have been carefully evaluated and isolated and it has been concluded that the amount of niobium in solution in the austenite is primarily responsible for the dramatic retardation. Alternative hypotheses to explain the mechanism whereby niobium exerts this effect on the hardenability of steel are discussed in detail. Soluble niobium reducing the austenite grain boundary energy is argued to be the most convincing explanation of the phenomenon and a reduction of grain boundary energy of $0.076 \mathrm{Jm}^{-2}$ per wt% of soluble niobium content has been proposed.

Keywords: soluble niobium, hardenability, transformation kinetics, grain boundary energy

1. Introduction

Niobium is recognised to have two principal roles in controlling the evolution of microstructure in thermomechanically processed steels. The first is in forming grain-boundary pinning-precipitates at temperatures where the steel is in its austenitic state, leading ultimately to a refined austenite grain size and all the advantages that this brings to the mechanical properties of the steel [1–3]. The second is the role of dissolved niobium in retarding recrystallisation and recovery during thermomechanical rolling and its subsequent influence on the hardenability of the steel [3–9]. It is the elucidation and quantification of the latter phenomenon with which the current work is concerned.

The influence of niobium on hardenability has been appreciated in the early work fifty years ago [4, 5]. The incubation time for the allotriomorphic ferrite transformation became longer in the niobium-containing steel as shown in the time–temperature–transformation (TTT) diagram, Fig. 1. Building on these early studies and further practical observations

on the processing of niobium treated steels Gray [3, 7] concluded that the effect of 0.05 wt% of Nb on hardenability was potentially as effective as about 1 wt% of Mn at a cooling rate of around $1^{\circ}Cs^{-1}$ and even more potent at faster cooling rates. Niobium has also been reported to retard the kinetics of transformations in a high-alloy (Fe-0.2C-10Cr-0.056Nb wt%) steel where the reactions involve the formation of large amount of chromium carbide in addition to ferrite [10].

The hardenability is not of course independent of the austenite grain size, and because of the ability of niobium rich precipitates to affect grain refining many researchers had difficulty in quantifying the relative contributions of grain size and soluble niobium. An early and well-cited study in this context is by Okaguchi et al. [11], who showed that the Ar_3 temperature where austenite first begins to transform into ferrite during cooling, decreased as the soluble niobium concentration was increased. However, they did not justify their use of information from titanium microalloyed steels to correct the Ar_3 data of niobium steels. Furthermore, there are significant inconsistencies in the Ar_3 temperatures for the titanium-containing steels, as can be seen by comparing their Figs 5 and 7. Nevertheless, their data for steels 1-3 as listed in Table 1, show that there is a substantial suppression of the transformation temperature in the presence of dissolved niobium. The comparison by Fossaert et al. (steels 4 and 5) is based on measured austenite grain sizes and soluble niobium concentrations, and proves that there is an intrinsic improvement of hardenability in the presence of dissolved niobium; many more details are available in the original publication [12]. Recent work [13] has indicated that at approximately constant austenite grain size, achieved in different steels by austenitisation at 1250°C for periods ranging from 5 to 300 s, the rate of austenite to ferrite transformation is slowest for the alloy containing 0.028 wt% Nb when compared with lower concentrations.

The discussion thus far has been in terms of hardenability with respect to the avoidance of allotriomorphic ferrite. A TTT diagram consists of two domains [14], defined by a C-curve at temperatures above approximately 600°C where phase changes that involve reconstructive diffusion [15] occur, for example, allotriomorphic ferrite and pearlite. At lower temperatures, displacive transformations are favoured, including Widmanstätten ferrite, bainite and martensite. The influence of hardenability enhancing solutes is different for these two kinds of transformation. The thermodynamic effect of alloying elements on the relative stabilities of austenite and ferrite is identical for all transformation products. However, the substitutional solutes do not partition during displacive transformation, whereas they may do so in the case of the reconstructive transformation products. This exaggerates the effect of alloying elements on the kinetics of reconstructive transformations. It is for this reason, that dissolved niobium has a rather small effect on the rate of the bainite reaction in contrast to allotriomorphic ferrite which is significantly retarded [16]. On the particular steel that the current study is concerned with, a delay of allotriomorphic ferrite transformation was demonstrated previously [17] by comparing the TTT diagrams obtained by isothermal transformation experiments and by calculation without considering the niobium effect.

It has been argued that niobium also increases the hardenability of TRIP-assisted alloys (steels 6,7, Table 1) [18]. These high-silicon steels have a mixed microstructure of allotriomorphic ferrite, bainite and retained austenite. The claim is that the amount of retained austenite increased in the niobium-alloyed variant, when the comparison is made at the same fraction of allotriomorphic ferrite and austenite condition. However there is no clear trend demonstrated as shown in Fig. 2, especially when it is considered that no uncertainties were stated in the measurement of the phase fractions. In other work where a niobium addition was claimed to enhance the retained austenite content of TRIP-assisted steel [19], the volume fractions of the other phases present were not reported. Since the partitioning of carbon into austenite is dependent on those fractions, it is difficult to conclude whether the observed changes in retained austenite are due to niobium in solution.

2. Hardenability Enhancement Mechanisms

The precise mechanism by which niobium enhances the hardenability of austenite can stand clarification [12, 20–24]. It is possible that the segregation of niobium and carbon into the austenite grain boundaries leads to a reduction in the activity of carbon, and that this causes a reduction of the gradient of carbon in the austenite [25]. However, this confuses the thermodynamics of the γ/γ interface with that in the unperturbed austenite ahead of a transformation front [26].

A reasonable explanation is that niobium segregates to the austenite grain surfaces and the resulting reduction in γ/γ interfacial energy per unit area makes the boundaries less potent nucleation sites. Indeed, there is some evidence to support a reduced nucleation rate [27, 28]. Recent atom-probe studies suggest this kind of segregation but find that the segregation is not limited to niobium [24]. Manganese, silicon, phosphorus and carbon were also demonstrated to be enriched in the austenite grain boundaries so the interpretation of the specific role of niobium becomes uncertain.

The situation becomes more complicated during the thermomechanical processing of austenite because the deformation-induced precipitation of Nb reduces the amount in solid solution. No increase of hardenability was found by continuous cooling of the steel with composition of Fe–0.04C–0.3Si–1.39Mn–0.037Al–0.41Ni–0.025Nb–0.014Ti wt% after 40–60% reduction and holding at 800°C for 5 min [29]. However significant lowering of Ar_3 was reported in a steel with composition of Fe–0.09C–0.25Si–1.45Mn–0.011Nb after 69% reduction at 800°C [30]. It is possible that there was no holding time provided for the precipitation after the deformation and before the continuous cooling in the latter work, but in both cases information was lacking on how much soluble Nb was available for retarding the transformation.

The retardation of the austenite to ferrite transformation has been reported during isothermal heat treatment, i.e., the transformation rate of the steel containing soluble Nb is slower compared to the Nb free steel with similar base composition [13, 31]. Consistent with

the earlier discussion, this retardation effect was greater for the diffusional transformation to allotriomorphic ferrite than in the displacive transformation to bainite.

It has been suggested that the effect that niobium has on retarding transformation is diminished when its concentration exceeds 0.04 wt% in alloys with base composition Fe–0.08C–1.39Mn–0.4Si–0.003S–0.039Al–0.006N wt% approximately [25]. The steels were austenitised at 1300°C for 5 min so that all the Nb was in solution, then helium quenched to 950°C just above Ac_3 and immediately cooled at various rates. It was proposed that with higher Nb content the Nb(C,N) readily precipitates during cooling, which promotes the ferrite transformation by generating more nucleation sites. This contradicts observations that Nb precipitation in recrystallised austenite is sluggish [32]. Only 40% of the total niobium content could be precipitated after holding a steel with the composition of Fe–0.062C–1.71Mn–0.12Si–0.074Nb–0.02Mo–0.006N–0.016P–0.011S wt% at 900°C for nearly 100 minutes.

Conversely, Yeo [33] studies the effect of alloying elements including niobium on the martensite-start (M_S) temperature of Fe-22.5Ni wt% alloys and found that the M_S decreased steadily with the increase of niobium concentration from 0.05 to 0.8 wt%. Quoting this work, Hanzaki and co-workers [19] stated that niobium reduces M_S whereas the original work show the opposite effect that at concentrations less than 0.05 wt%, the niobium-containing alloys had a greater M_S than the niobium-free samples. The concentration used in this case was only 0.035 wt%. It can be surmised therefore, that the role of niobium in enhancing hardenability cannot be on the thermodynamic stability of the austenite.

It has been speculated [19, 34, 35] that carbide–forming elements such as Mo, Nb and V retard the diffusion of carbon during the transformation from austenite to ferrite. The calculations in Table 2, done using *DICTRA* [36] and associated mobility databases, show that this notion is not justified, and where that the variations are insignificantly small [37].

Diffusion features in another context when explaining the hardenability change due to niobium additions. Solute drag and 'solute drag like effects' are sometimes said to enhance hardenability [19]. Solute drag arises when free energy is dissipated when segregated-solute diffuses within a moving interface, and this motion may induce diffusion profiles in the vicinity of the interface, where these latter profiles are not to be confused with the partitioning of solute between phases [38, 39]. There is no theoretical framework for solute-drag like effects, originally proposed to explain discrepancies in growth rate data for allotriomorphs of ferrite [40]. The logic of the proposed drag-like effect has been critically assessed [26]. But it is important to note, as pointed out by DeArdo et al. [41] tracer diffusion data show that the interdiffusion coefficient of niobium in austenite is significantly larger than the self-diffusion coefficient for iron. If this can be extrapolated to an α/γ interface then significant drag effects due to niobium diffusion in the interface are not likely given that iron atoms have to diffuse during diffusional transformations [15]. Some of the speculation is related to the effect of niobium on reducing the activity of carbon in austenite, a well-established fact [42]. This thermodynamic effect is fully accounted for in equilibrium phase diagrams, and as shown later in the paper, it is of minor consequence.

The goal of the present work was to study the transformation behavior of a commercial high temperature processed steel which has been in service since 2004. The steel has a Nb/C ratio significantly higher than that traditionally associated with pipeline steels but this now represents a tried and tested concept which has been applied in large scale pipeline projects all over the world and which is likely to find application in the structural sector for both flat and long products. To assist in alloy designs involving new areas of applications, it would be useful to have a quantitative expression of the soluble niobium effect on transformation kinetics.

3. Experimental Procedures

The steel studied has a chemical composition listed in Table 3 and is the original alloy used in the Cheyenne Plains X80 steel pipeline project [43]. Heat treatments were carried out in a THERMECMASTER thermomechanical simulator using cylindrical samples of diameter 8 mm height of 12 mm along the normal to the steel plate. Continuous cooling heat treatments were carried out by austenitising the specimens at 1260°C for 1 min and 960°C for 5 min and quenching to room temperature at various cooling rates. In the industrial process, the former is the peak holding temperature used for austenitisation and the latter is the intermediate holding temperature applied before the final stage of the hot rolling.

Metallographic samples were ground using sand paper, polished with diamond paste and then etched with 3% nital, followed by characterisation using a Zeiss Axiotech optical microscope. Microhardness measurements were carried out on the etched surfaces using a Mitutoyo microhardness tester with a load of 300 gF and dwell time of 10 s.

The prior austenite grain boundaries were revealed by the thermal etching method [44]. The samples were polished to a 1 μm finish, followed by cleaning with ethanol during ultrasonic agitation. The samples were then heated to 960°C and held for 5 min, to 1160°C held for 6 s, and to 1260°C held for 1 min in the thermomechanical simulator under vacuum. Helium quenching was applied after the former two austenitisation conditions. Another sample was sealed in a quartz tube, put into a preheated box furnace at 960°C for 24 h and finally quenched with liquid nitrogen. The prior austenite grain boundaries were then detectable because of the formation of allotriomorphic ferrite along them. The thermal etching method could not be used in this case because of the oxidation and complications associated with long holding time [44]. The prior austenite grain size was measured quantitatively by linear intercept method. Another set of samples were also applied the above mentioned 4 kinds of austenitisation conditions and identical cooling rate of $20^{\circ}\mathrm{C\,s^{-1}}$ in the thermomechanical simulator to check the transformation start temperatures.

4. Results and Discussion

The retardation of austenite to allotriomorphic ferrite transformation in the X80 steel is demonstrated by continuous cooling at a range of rates after austenitisation at 1260 and

960°C respectively, Fig. 3. After austenitisation at 1260°C for 1 min, the transformations happened in a narrow temperature range which is between 446 and 494°C at the highest cooling rate of 86°C s^{-1} and 564–609°C at the slowest cooling rate of 0.5°C s^{-1} (Fig. 3a). The martensite start temperature (M_S) is 464°C, and between 500 and 600°C is the bainite transformation region of the X80 steel, the transformation mechanism of which is described elsewhere [17]. The samples therefore transformed to a mixture of bainite and martensite upon the whole range of cooling rate, which is consistent with the plate-like microstructure as shown in Fig. 4. Hardness measurements of these continuously-cooled samples are shown in Fig. 5. The decrease of hardness with the cooling rate can be explained by the coarsening of the bainite plates. Possibly there is also a small amount of allotriomorphic ferrite existing in the samples cooled slower than 5°C s^{-1} because of the significant drop of hardness and the transformation start temperature being slightly higher than 600°C.

In comparison, the transformations happened in a much wider temperature range, more than 100°C, after austenitisation at 960°C for 5 min. The transformation-start temperatures exceeded 600°C except at the highest cooling rates of 60°C s^{-1}, which suggests the formation of allotriomorphic ferrite, as confirmed metallographically (Fig. 6). This is consistent with the lower hardness values of these samples relative to those cooled from 1260°C.

There is obviously a substantial delay in the onset of allotriomorphic ferrite when cooling the X80 steel from 1260°C. Thermal etching was used to reveal the equiaxed-austenite grain sizes, *cf.* Fig. 7a and 7b. Allotriomorphic ferrite formation should be suppressed by the larger prior austenite grain size associated with the 1260°C heat treatment.

When the samples were heated to different austenitisation temperatures the soluble niobium contents are expected to be different. The alloy design of this steel is based on the concept that titanium predominantly combines with most of the nitrogen at temperatures higher than the austenitisation temperature of 1260°C, which facilitates the niobium to go into solution and precipitate with carbon at lower temperatures [45]. The amount of soluble niobium in the steel can be estimated using the solubility product for niobium carbide which is given by [46]:

$$\log[\mathrm{Nb}][\mathrm{C}]^{0.87} = -\frac{7520}{T} + 3.11 \tag{1}$$

where [Nb] and [C] are the wt% in solution within the steel, and T is the absolute temperature. The Nb–C solubility diagram is illustrated in Fig. 8. When the sample is heated to 1260°C, all the niobium is in solid solution, so the soluble niobium content is the same as the alloying composition in the steel, 0.095 wt%. In comparison there is only 0.016 wt% of soluble niobium at the austenitisation temperature of 960°C according to the solubility calculation (Fig. 8). The excess of 0.079 wt% of soluble niobium at the austenitisation temperature of 1260°C also plays an important role in retarding the allotriomorphic ferrite transformation in the steel as confirmed by the relation between transformation start temperature and the prior austenite grain size at different austenitisation conditions shown in Fig. 9.

Comparing the samples austenitised at T_γ = 960°C for 5 min and at 1260°C for 1 min,

the prior austenite grain sizes are around 10 and 70 μm respectively. The difference between the transformation start temperatures of the two samples at same cooling rate of $20°C\,s^{-1}$ is nearly 100°C, Fig. 9. After the sample is heated at 960°C for 24 h, the transformation start temperature decreases from 651°C to 613°C with the increase of prior austenite grain size from around 10 μm to nearly 30 μm. The longer time at T_γ provides more time for the dissolution of niobium carbides, to the equilibrium value of 0.016 wt%. The sample with $T_\gamma = 1160°C$ for 6 s has a similar prior austenite grain size of $\approx 30\,\mu m$ (Fig. 9). The solubility limit of niobium carbide at 1160°C is just above the alloying content of the X80 steel shown in Fig. 8, so there is possibly a small amount of NbC pinning the austenite grain boundaries, which leads to a significant drop of prior austenite grain size compared to the sample austenitised at 1260°C where all the NbC is dissolved. This is the classic grain growth behaviour of niobium microalloyed steel [12]. There should be nearly 0.079 wt% more soluble niobium in the sample austenitised at 1160°C compared to that austenitised at 960°C for 24 h, which suppresses the transformation start temperature down 40°C. In summary, the results in Fig. 9 show conclusively the role of dissolved niobium in retarding the allotriomorphic ferrite transformation at the same austenite grain size.

Thermodynamic calculations were carried out to assess the idea that the hardenability effect of niobium is via its influence on the activity of carbon in austenite [25]. The activity was calculated for the alloy composition (Table 3) with or without the niobium, Fig. 10. The reduction of carbon activity due to 0.095 wt% of Nb content is 2% between 600 and 800°C, which is equivalent to the effect of 0.001 wt% change of the carbon content (0.05 wt%×0.02).

As mentioned earlier, the most convincing explanation is that niobium segregates to the austenite grain boundaries and reduces the austenite grain boundary energy ($\sigma_{\gamma\gamma}$). This is important because the destruction of a portion of grain boundary during the heterogeneous nucleation of ferrite leads to a dramatic reduction in the activation energy for nucleation [47]. Nucleation of course involves the creation of ferrite/austenite interfaces, and if these have an energy per unit area of $\sigma_{\alpha\gamma}$ then the net change during heterogeneous nucleation will be related approximately to $a\sigma_{\alpha\gamma} - b\sigma_{\gamma\gamma} > 0$ where a and b depend on the details of the nucleus shape and the balancing of interfacial tensions. According to classic nucleation theory, the nucleation rate of allotriomorphic ferrite, I, is given by:

$$I = C_a \frac{kT}{h} \exp\left\{-\frac{G^* + Q}{RT}\right\} \exp\left\{-\frac{\tau^*}{t}\right\} \tag{2}$$

where h is the Plank constant, k is the Boltzmann constant, $C_a = 1.214 \times 10^{12}\,m^{-2}$ is a constant related to the number of atoms on a grain boundary that serve as a single nucleation site, in other words, it defines the number of nucleation sites per unit area of boundary [48], R is the universal gas constant and $Q = 200\,kJ/mol$ is the energy barrier to transfer atoms across the α/γ interface, t is the transformation time. It follows that the significant term in the effect of niobium on nucleation kinetics is

$$I \propto \exp\{-G^*/kT\} \propto \exp\{-(a\sigma_{\alpha\gamma} - b\sigma_{\gamma\gamma})^3/kT\} \tag{3}$$

The activation energy for nucleation, G^*, is proportional to the cube of the interfacial energy Σ,

$$G^* = \frac{C_b \Sigma^3}{\Delta G^2} \tag{4}$$

where $C_b = 5.58$ is another fitted constant and ΔG is the maximum chemical free energy change per unit volume available for nucleation [49]. If $\Sigma = a\sigma_{\alpha\gamma} - b\sigma_{\gamma\gamma}$ then a larger value of Σ makes heterogeneous nucleation more difficult. Therefore, if niobium segregation leads to a reduction $\Delta\sigma$ in $\sigma_{\gamma\gamma}$ then Σ would increase, leading to a retardation in the nucleation rate. For a steel containing dissolved niobium, the term can be approximated as

$$\Sigma = a\sigma_{\alpha\gamma} - [b\sigma_{\gamma\gamma} - x_{\mathrm{Nb}}\Delta\sigma] \tag{5}$$

where x_{Nb} is the concentration of soluble niobium capable of segregating to the interface and the term $\Delta\sigma$ is to be found by fitting to experimental data. The second exponential term in equation 2 relates to the achievement of a steady-state nucleation rate:

$$\tau^* = \frac{n_c^2 h}{4 a_c k T} \exp\left\{\frac{Q}{RT}\right\} \tag{6}$$

where n_c is the number of atoms in the critical nucleus and a_c is the number of atoms in the critical nucleus at the interface [47].

To model the transformation requires theory capable of taking nucleation, growth and impingement between particles growing from different regions, together with soft-impingement due to the enrichment of carbon in residual austenite, to be taken into account. Such theory is based on the Cahn model [50], which unlike the Johnson-Mehl-Avrami theory deals with non-random nucleation at grain boundaries. It requires therefore, two integrations over extended space, the first dealing with impingement parallel to the boundaries, and the second impingement between particles nucleated at different grain boundaries. The allotriomorphic ferrite can be modelled as discs having their faces parallel to the nucleating grain boundary plane. The transformation is described by an equation of the form:

$$-\ln\{1-\chi\} = \frac{2 S_V \alpha_1 \sqrt{t}}{\phi} f\{\theta, \eta\alpha_1, I, t\} \tag{7}$$

with

$$f\{\theta, \eta\alpha_1, I, t\} = \int_0^1 (1 - \exp\{-0.5\pi I(\eta\alpha_1)^2 t^2 [1-\theta^4]\})\, d\theta \tag{8}$$

where χ is the actual volume fraction of allotriomorphic ferrite normalised by the equilibrium fraction:

$$\chi = \frac{V_\alpha}{V\phi} \tag{9}$$

ϕ is dependent on the phase diagram and ensures that the fraction of transformation never exceeds that expected from equilibrium,

$$\phi = \frac{x^{\gamma\alpha} - \bar{x}}{x^{\gamma\alpha} - x^{\alpha\gamma}} \tag{10}$$

where $x^{\gamma\alpha}$ and $x^{\alpha\gamma}$ is the equilibrium or paraequilibrium C content of austenite and ferrite, $\bar{x}$ is the average C content of the alloy. S_V is the amount of austenite grain boundary area per unit volume, η is the aspect ratio of the allotriomorphic ferrite, $\theta = y/\alpha_1\sqrt{t}$, y is the distance between the nucleating boundary and an arbitrary plane parallel to the boundary (to help account for impingement between particles nucleating from different boundaries), and α_1 is a parabolic rate constant describing the growth of the ferrite, which is obtained by solving the equation:

$$2\sqrt{\frac{\underline{D}}{\pi}}\phi = \alpha_1 \exp\left\{\frac{\alpha_1^2}{4\underline{D}}\right\} \operatorname{erfc}\left\{\frac{\alpha_1}{2\sqrt{\underline{D}}}\right\} \tag{11}$$

where D is the diffusivity of carbon in austenite at a particular concentration of carbon. $\underline{D}$ is a weighted average diffusivity of carbon in austenite, given by:

$$\underline{D} = \int_{x^{\gamma\alpha}}^{\bar{x}} \frac{D\{x\}}{\bar{x} - x^{\gamma\alpha}}\, dx \tag{12}$$

The classic theory is extended to not only allotriomorphic ferrite but also pearlite, Widmanstätten ferrite and bainite. The gradual development of microstructure in the steel undergoes simultaneous transformations can be modelled by dividing the calculation into time steps. The full concepts including continuous cooling transformation, are published elsewhere [48, 51] and implemented in freely available, documented computer programs [52]. The important point here is that the interfacial energy is an input into this model and the effect of niobium can in principle be taken into account by using Σ (equation 5) as the effective interfacial energy. Calculations were carried out using Σ as a fitting parameter to match the volume fraction of allotriomorphic ferrite obtained under different conditions.

The average prior austenite grain size as shown in Fig. 9 measured by linear intercept ($\equiv 2/S_V$) is an input into the program, and calculations were carried out down to 600°C during continuous cooling at the appropriate rates, since allotriomorphic ferrite gives way to bainite at about that temperature and experiments show that it forms above this temperature [17]. The volume fractions of allotriomorphic ferrite thus obtained are listed in Table 4. It is emphasised that the calculations account for alloying elements (C, Mn, Si, Ni, Cr), the cooling rate and the austenite grain size.

When the samples are cooled after austenitisation at 960°C for 5 min, the calculations show that allotriomorphic ferrite forms at all cooling rates and the amount increases with decrease of the cooling rate as shown in Table 4a. The γ/α interfacial energy of 0.03 $\mathrm{Jm^{-2}}$

was fitted with the calculated transformation start temperatures in agreement with the experimental results under cooling rate below $20^{\circ}\mathrm{C\,s^{-1}}$, when the resultant microstructure contains a large amount of allotriomorphic ferrite. If only the increase of γ grain size is considered but not the increase of Σ for the samples cooled after austenitisation at 1260°C for 1 min, then allotriomorphic ferrite was calculated to be suppressed only at very high cooling rates of $60^{\circ}\mathrm{C\,s^{-1}}$, which is inconsistent with the experimental results. The transformation start temperatures are all below 600°C at cooling rates higher than $5^{\circ}\mathrm{Cs^{-1}}$ measured by the thermomechanical simulator (Fig. 3a), and the optical micrographs show the plate-like structure, Fig. 4c–4e. Thus $0.006\,\mathrm{Jm^{-2}}$ increase in Σ was used in account for 0.079 wt% more soluble niobium, giving

$$\Delta\sigma = \frac{0.006}{0.079} = 0.076\,\mathrm{J\,m^{-2}\,(wt\%\ of\ soluble\ niobium)^{-1}} \tag{13}$$

The allotriomorphic ferrite transformation was further suppressed to cooling rate lower than $5^{\circ}\mathrm{C\,s^{-1}}$, which is consistent with the experimental observation as shown in Fig. 3–6.

For the samples cooled at $20^{\circ}\mathrm{C\,s^{-1}}$, increasing the γ grain size due to the long austenitisation time of 24 h at 960°C retards the allotriomorphic ferrite formation to some extent as shown in Table 4b. Maintaining the γ grain size level and increasing the Σ interfacial energy due to the 0.079 wt% more soluble niobium content at austenitisation temperature of 1160°C and above suppresses the allotriomorphic ferrite transformation completely, which is consistent with the transformation start temperature lower than 600°C determined by dilatometry as shown in Fig. 9.

Calculations were carried out further in order to compare the effect of soluble amount of Nb and the alloy content of Mn on reducing the allotriomorphic ferrite transformation start temperature as shown in Fig. 11. The input parameters used in the calculation match the condition of cooling at $20^{\circ}\mathrm{Cs^{-1}}$ after austenitisation at 1260°C for 1 min, so the γ grain size of 70 μm is used. The alloy element contents of C, Mn, Si, Ni and Cr which are accounted for in the calculation are obtained from Table 3. For calculation of the soluble niobium effect on retarding the allotriomorphic ferrite transformation, the Mn content used is 1.55 wt%. Σ is set in a range from 0.029 to $0.036\,\mathrm{Jm^{-2}}$ corresponding to the soluble niobium content from 0.003 to 0.095 wt%. The soluble niobium content above 0.069 wt% corresponding to Σ above $0.034\,\mathrm{Jm^{-2}}$ is not plotted in Fig. 11, because the allotiomorphic ferrite transformation is completely suppressed and the transformation start temperature falls below 600°C. The effect of Mn content on transformation has already been taken into account in the kinetics calculation [48, 51]. The resultant allotriomorphic ferrite transformation start temperatures with increasing Mn content from the 1.55 to 2.05 wt% are plotted in Fig. 11. Σ of $0.029\,\mathrm{Jm^{-2}}$ representing 0.003 wt% of soluble Nb is used in these calculations. To summarise the result, on the base composition of Fe–0.05C–1.55Mn-0.12Si–0.13Ni–0.23Cr wt% adding nearly 0.07 wt% of soluble niobium shows the similar effect as increasing the Mn content of 0.5 wt% on reducing the allotriomorphic ferrite transformation start temperature nearly

50°C. Gray [3] suggested that 0.05 wt% niobium in solution can depress the γ to α transformation temperature to the same extent as 1 wt% Mn, but the current work provides an unambiguous assessment as any influence of grain refinement has been taken account of.

5. Conclusions

CCT diagrams were constructed after austenitisation at 1260 and 960°C in the X80 steel with high Nb/C ratio. A significant increase of hardenability at the austenitisation temperature high enough to dissolve all the niobium is demonstrated by both experimental results and calculation. The study separated the effect of higher soluble niobium from the larger prior austenite grain size and showed nearly 0.079 wt% higher concentration of soluble niobium lowered the Ar_3 40°C at cooling rate of $20^{\circ}\mathrm{C\,s^{-1}}$ and prior austenite grain size of $\sim$30 µm obtained by austenitising the steel at 1160°C for 6 s and 960°C for 24 h respectively. The mechanism of soluble niobium retarding the allotriomorphic ferrite transformation is most likely to be that niobium segregates to the prior austenite grain boundaries and reduces the austenite grain boundary energy. $\Delta\sigma$ is calculated at $0.076\,\mathrm{J\,m^{-2}}$ per wt% of soluble niobium.

There has been tremendous progress in the development and commercial exploitation of high-niobium, low-carbon pipelines, where niobium not only plays a crucial role during thermomechanical processing, but also provides the hardenability that is essential in compensating for the low carbon concentrations [43, 53, 54]. These pipe materials, because of their weldability, mechanical properties and cost are so successful that some six million tonnes have now been installed in service. The commercial goal now is to see whether the same low-carbon, high-niobium concept can be implemented in other applications such as construction steels used for high-rise buildings and other civil engineering applications where the high strength experienced in the pipe steels can lead to a reduction in weight and hence better engineering design. The present work, in particular the quantitative treatment of the niobium hardenability effect, can in principle be exploited to design such steels since they have different base compositions and processing requirements to pipe alloys. In particular, the work makes it is possible to account for niobium in the presence of multiple solutes such as manganese, silicon, nickel, chromium, molybdenum and vanadium.

Acknowledgements The authors are grateful to CBMM for financial support and for providing the steel, and would like to thank Drs Bob Keown, Philip Kirkwood and Malcolm Gray for helpful discussions. They also thank Professor A. L. Greer for the provision of laboratory facilities at the University of Cambridge.

References

1. T. Gladman: The Physical Metallurgy of Microalloyed Steels: IOM Communications, London, 1996.

2. W. B. Morrison: 'Microalloy steels – the beginning', *Materials Science and Technology*, 2009, **25**, 1066–1073.

3. J. M. Gray: 'Effect of niobium (columbium) on transformation and precipitation processes in high strength low alloy steels', In: *Heat Treatment '73*. London, U.K.: Metals Society, 1973:19–28.

4. L. Rönn: 'Niobs inverkan på TTT-diagrammet av ett mjukt stål': 1963.

5. F. de Kazinczy, A. Axn´as, and P. Pachleitner: 'Some properties of niobium-treated mild steel', *Jernkontorets Annaler*, 1963, **147**, 408–433.

6. G. L. Fisher, and R. H. Geils: 'The effect of columbium on the alpha-gamma transformation in a low alloy Ni-Cu steel', *Trans. Metall. Soc. AIME*, 1969, **245**, 2405–2412.

7. J. M. Gray: 'Metallurgy of high-strength low-alloy pipeline steels: present and future possibilities': Tech. Rep. 7201, Molycorp, 1972.

8. T. Tanaka: 'Controlled rolling of steel plate and strip', *International Metals Reviews*, 1981, **4**, 185–212.

9. G. T. Eldis, and W. C. Hagel: 'Effects of microalloying on the hardenability of steels', In: D. V. Doane, and J. S. Krikaldy, eds. *Hardenability concepts with applications to steels*. Warrendale, Pennsylvania, USA: TMS-AIME, 1977:397–415.

10. P. R. Rios, and R. W. K. Honeycombe: 'Effect of niobium on decomposition of austenite in 0.2C-10Cr steel', *Materials Science and Technology*, 1992, **8**, 1057–1062.

11. S. Okaguchi, T. Hashimoto, and H. Ohtani: 'Effect of niobium, vanadium and titanium on transformation behavior of HSLA steel in accelerated cooling', In: *Physical Metallurgy of Thermomechanical Processing of Steels and Other Metals*, vol. 1. Tokyo, Japan: Iron and Steel Institute of Japan, 1988:330–336.

12. C. Fossaert, G. Rees, T. Maurickx, and H. K. D. H. Bhadeshia: 'The effect of niobium on the hardenability of microalloyed austenite', *Metallurgical and Materials Transactions A*, 1995, **26A**, 21–30.

13. L. Wang, S. Parker, A. Rose, G. West, and R. Thomson: 'Effect of niobium on transformations from austenite to ferrite in low carbon steels', In: *Proceedings of the 6th International Conference on High Strength Low Alloy Steels*. 2011:208–212.

14. H. K. D. H. Bhadeshia: 'A thermodynamic analysis of isothermal transformation diagrams', *Metal Science*, 1982, **16**, 159–165.

15. H. K. D. H. Bhadeshia: 'Diffusional formation of ferrite in iron and its alloys', *Progress in Materials Science*, 1985, **29**, 321–386.

16. G. I. Rees, J. Perdrix, T. Maurickx, and H. K. D. H. Bhadeshia: 'The effect of niobium in solid solution on the transformation kinetics of bainite', *Materials Science and Engineering A*, 1995, **194**, 179–186.

17. P. Yan, and H. K. D. H. Bhadeshia: 'Mechanism and kinetics of solid-state transformation in high-temperature processed linepipe steel', *Metallurgical & Materials Transactions A*, 2013, **44**, 5468–5477.

18. E. V. Pereloma, I. B. Thimokhina, and P. D. Hodgson: 'Transformation behaviour in thermomechanically processed C-Mn-Si TRIP steels with and without Nb', *Materials Science & Engineering A*, 1999, **273-275**, 448–452.

19. A. Z. Hanzaki, P. D. Hodgson, and S. Yue: 'Retained austenite characteristics in thermomechanically processed Si-Mn transformation-induced plasticity steels', *Metallurgical and Materials Transactions A*, 1997, **28**, 2405–2414.

20. Y. Li, D. N. Crowther, M. J. W. Green, P. S. Mitchell, and T. N. Baker: 'The effect of vanadium and niobium on the properties and microstructure of the intercritically reheated coarse grained heat affected zone in low carbon microalloyed steels', *ISIJ International*, 2001, **41**, 46–55.

21. A. J. DeArdo: 'Fundamental metallurgy of niobium in steel', In: *Proceedings of the International Symposium Niobium 2001, Florida*. Warrendale, Pennsylvania, USA: TMS, 2001:427–278.

22. S. Yamamoto, C. Ouchi, and T. Osuka: 'The effect of microalloying elements on the recovery and recrystallization in deformed austenite', In: A. J. DeArdo, G. A. Ratz, and P. J. Wray, eds. *Thermomechanical processing of microalloyed austenite*. Pittsburgh, USA: TMS-AIME, 1981:613–639.

23. P. R. Kirkwood: 'Niobium and heat-affected zone mythology': Tech. Rep., http://www.apia.net.au/, U. K., 2011.

24. P. J. Felfer, C. R. Killmore, J. G. Williams, K. R. Carpenter, S. P. Ringer, and J. M. Cairney: 'A quantitative atom probe study of the Nb excess at prior austenite grain boundaries in a Nb microalloyed strip-cast steel', *Acta Materialia*, 2012, **60**, 5049–5055.

25. M. H. Thomas, and G. M. Michal: 'The influence of niobium and Nb(C,N) precipitation on the formation of proeutectoid ferrite in low alloy steels', In: H. I. Aaronson, D. E. Laughlin, R. F. Sekerka, and C. M. Wayman, eds. *Proceedings of an international conference on solid-solid phase transformation*. TMS-AIME, 1981:469–473.

26. H. K. D. H. Bhadeshia: 'Considerations of solute drag in relation to transformations in steels', *Journal of Material Science*, 1983, **18**, 1473–1481.

27. C. Ouchi, T. Sampei, and I. Kozasu: 'The effect of hot rolling condition and chemical composition on the onset temperature of γ/α transformation after hot rolling', *Transactions of the Iron and Steel Institute of Japan*, 1982, **22**, 214–222.

28. M. Enomoto, N. Nojiri, and Y. Sato: 'Effects of vanadium and niobium on the nucleation kinetics of pro-eutectoid ferrite at austenite grain boundaries in Fe-C and Fe-C-Mn alloys', *Materials Transactions, JIM*, 1994, **35**, 859–867.

29. K. Abe, M. Shimizu, S. Takashima, and H. Kaji: 'Metallurgical meenings of niobium addition in the formation of acicular ferrite in low carbon steel manufactured by accelerated cooling process', In: I. Tamura, ed. *International Conference on Physical Metallurgy of Thermomechanical Processing of Steels and Other Metals*, vol. 1. Tokyo, Japan: Iron and Steel Institute of Japan, 1988:322–329.

30. T. Abe, K. Tsukada, and I. Kozasu: 'Role of interrupted accelerated cooling and microalloying on weldable HSLA steels', In: J. M. Gray, T. Ko, S. Zhang, B. Wu, and X. Xie, eds. *HSLA Steels: Metallurgy and Applications*. Metals Park, Ohio, USA: ASM International, 1985:103–111.

31. R. K. Amin, and F. B. Pickering: 'Ferrite formation from thermo-mechanically processed austenite', In: A. J. DeArdo, G. A. Ratz, and P. J. Wray, eds. *Thermomechanical processing of microalloyed austenite*. Pittsburgh, USA: TMS-AIME, 1981:377–403.

32. H. Watanabe, Y. E. Smith, and R. D. Pehlke: 'Precipitation kinetics of niobium carbonitride in austenite of high-strength low-alloy steels', In: J. B. Ballance, ed. *The Hot Deformation of Austenite*. New York: American Institute of Mining, Metallurgical and Petroleum Engineers, Inc., 1977:140–168.

33. R. B. G. Yeo: 'Effects of some alloying elements on the transformation of Fe-22.5Ni wt% alloys', *Trans. Metall. Soc. AIME*, 1963, **227**, 884–890.

34. H. Tamehiro, K. Nishioka, M. Murata, R. Habu, and Y. Kawada: 'Properties of high toughness X80 line pipe steels', In: *Int. Symposium on Accelerated Cooling of Rolled Steel*. Winnipeg, Canada: Canadian Institute of Metals, 1987:1–8.

35. F. Matsuda, Y. Fukada, H. Okada, C. Shiga, K. Ikeuchi, Y. Horii, T. Shiwaku, and S. Suzuki: 'Review of mechanical and metallurgical investigations of martensite-austenite constituent in welded joints in Japan', *Welding in the World*, 1996, **37**, 134–154.

36. J. O. Andersson, T. Helande, L. Hoglund, P. Shi, and B. Sundman: 'Thermo-Calc & DICTRA, computational tools for materials science', *CALPHAD*, 2002, **26**, 273–312.

37. H. K. D. H. Bhadeshia: 'About calculating the characteristics of the martensite-austenite constituent', In: *Welding of High Strength Pipeline Steels*. Metals Park, Ohio, USA: TMS, 2013:99–106.

38. J. W. Cahn: 'The impurity drag effect in grain boundary motion', *Acta Metallurgica*, 1962, **10**, 789–798.

39. M. Hillert: 'The role of interfaces in phase transformations', In: *Mechanism of Phase Transformations in Crystalline Solids*. Monograph and Report Series No. 33, London, U.K.: Institute of Metals, 1970:231–247.

40. J. R. Bradley, and H. I. Aaronson: 'Growth kinetics of grain boundary ferrite allot. in Fe-C-X alloys', *Metallurgical Transactions A*, 1981, **12**, 1729–1741.

41. A. J. Deardo, J. M. Gray, and L. Meyer: 'Fundamental metallurgy of niobium in steel', In: H. Stuart, ed. *Niobium '81*. Warrendale, Pennsylvania, USA: TMS-AIME, 1981:685–759.

42. R. C. Sharma, V. K. Lakshmanan, and J. S. Kirkaldy: 'Solubility of NbC and NbCN in alloyed austenite and ferrite', *Metall. Trans. A*, 1984, **15**, 545–553.

43. D. Stalheim: 'The use of high temperature processing (HTP) for high strength oil and gas transmission pipeline applications', In: *Proceedings of the 5th HSLA Steels Conference, Iron and Steel Supplement*, vol. 40. 2005:699–704.

44. M. J. Day, and J. B. Austin: 'Heat etching as a means of revealing austenite grain size', *Trans. ASM*, 1940, **28**, 354–371.

45. H. Zou, and J. S. Kirkaldy: 'Thermodynamic calculation and experimental verification of the carbonitride-austenite equilibrium in Ti-Nb microalloyed steels', *Metall. Trans. A*, 1992, **23A**, 651–657.

46. H. Nordberg, and B. Aronsson: 'Solubility of niobium carbide in austenite', *Journal of the Iron and Steel Institute*, 1968, **206**, 1263–1266.

47. J. W. Christian: Theory of Transformations in Metals and Alloys, Part I: 3 ed., Oxford, U. K.: Pergamon Press, 2003.

48. S. Jones, and H. K. D. H. Bhadeshia: 'Kinetics of the simultaneous decomposition of austenite into several transformation products', *Acta Materialia*, 1997, **45**, 2911–2920.

49. M. Hillert: 'Role of interfacial energy during solid-state phase transformations', *Jernkontorets Annaler*, 1957, **141**, 757–789.

50. J. W. Cahn: 'The kinetics of grain boundary nucleated reactions', *Acta Metallurgica*, 1956, **4**, 449–459.

51. H. K. D. H. Bhadeshia, L.-E. Svensson, and B. Gretoft: 'Theory for allotriomorphic ferrite formation in steel weld deposits', In: J. Y. Koo, ed. *Welding Metallurgy of Structural Steels*. Warrendale, Pennsylvania, USA: TMS-AIME, 1987:517–530.

52. U. of Cambridge, and NPL: 'Materials Algorithms Project, www.msm.cam.ac.uk/map/mapmain.html': 2013: URL `www.msm.cam.ac.uk/map/mapmain.html`.

53. K. Hulka, F. Heisterkamp, and L. Hachtel: 'Correlation of processing, microstructure and mechanical properties in 0.03-0.1 wt% Nb steel', In: A. J. DeArdo, ed. *Processing, Microstructure and Properties of HSLA Steels*. Warrendale, Pennsylvania, USA: TMS-AIME, 1988:153–167.

54. K. Hulka, and J. M. Gray: 'High-temperature processing of line-pipe steels', In: *Niobium 2001*. Warrendale, Pennsylvania, USA: TMS-AIME, 2001:587–612.

55. H.-S. Yang, and H. K. D. H. Bhadeshia: 'Uncertainties in the dilatometric determination of the martensite-start temperature', *Materials Science and Technology*, 2007, **23**, 556–560.

56. NPL: 'MTDATA': Software, National Physical Laboratory, Teddington, U.K., 2006.

Table 1: The concentrations are in wt%, and [Nb] represents niobium dissolved in austenite. $\dot{T}$ is a cooling rate, and $\dot{T}_C$ a critical cooling rate to obtain 95% martensite. The austenite grain size index d_γ is larger when the size is smaller. Data from [11].

Steel	C	Si	Mn	Nb	$\dot{T}/^\circ\mathrm{C\,s^{-1}}$	$Ar_3/^\circ\mathrm{C}$	Reference
1	0.10	0.24	1.49	-	5	739	[11]
1	0.10	0.24	1.49	-	10	680	[11]
2	0.10	0.26	1.50	0.02	5	719	[11]
2	0.10	0.26	1.50	0.02	10	646	[11]
3	0.10	0.26	1.50	0.04	5	701	[11]
3	0.10	0.26	1.50	0.04	10	628	[11]

Steel	C	Si	Mn	Nb	$\dot{T}_C/^\circ\mathrm{C\,s^{-1}}$	d_γ	Reference
4	0.178	0.023	1.527	-	80	7.5	[12]
5	0.152	0.467	1.545	0.035	30	7.5	[12]
4	0.178	0.023	1.527	-	45	4	[12]
5	0.152	0.467	1.545	0.035	30	4	[12]

Steel	C	Si	Mn	Nb			Reference
6	0.2	1.5	1.5	0.039			[18]
7	0.2	1.5	1.5	-			[18]

Table 2: Influence of niobium on the diffusivity of carbon in austenite at 1000°C.

Composition / wt%	Diffusivity $\mathrm{m^2\,s^{-1}}$
Fe-0.1C	2.25011×10^{-11}
Fe-0.1C-0.5Nb	2.25094×10^{-11}
Fe-0.1C-0.5Mo	2.25016×10^{-11}
Fe-0.1C-0.5Mn	2.24938×10^{-11}

Table 3: Chemical composition, wt%

C	Mn	P	S	Si	Cu	Ni
0.05	1.55	0.012	0.002	0.12	0.24	0.13
Nb	Al	Cr	Ti	N	Ca	
0.095	0.037	0.23	0.011	0.0033	0.0012	

Table 4: Allotriomorphic ferrite volume fraction calculated using kinetic theory [48, 51].

(a) Samples continuously cooled at different cooling rates

Austenisation	γ grain size / μm	Σ/J m^{-2}	60°C s^{-1}	20°C s^{-1}	5°C s^{-1}
			Volume fraction of ferrite		
960°C for 5 min	11	0.03 Jm^{-2}	0.016	0.406	0.741
1260°C for 1 min	70	0.03 Jm^{-2}	< 0.01	0.092	0.241
		0.036 Jm^{-2}	< 0.01	< 0.01	0.139

(b) Samples continuously cooled at 20°C s^{-1}

Austenisation	γ grain size / μm	Σ/J m^{-2}	Volume fraction of ferrite
960°C for 5 min	11	0.03	0.406
960°C for 24 h	26	0.03	0.219
1160°C for 6 s	29	0.036	< 0.01
1260°C for 1 min	70	0.036	< 0.01

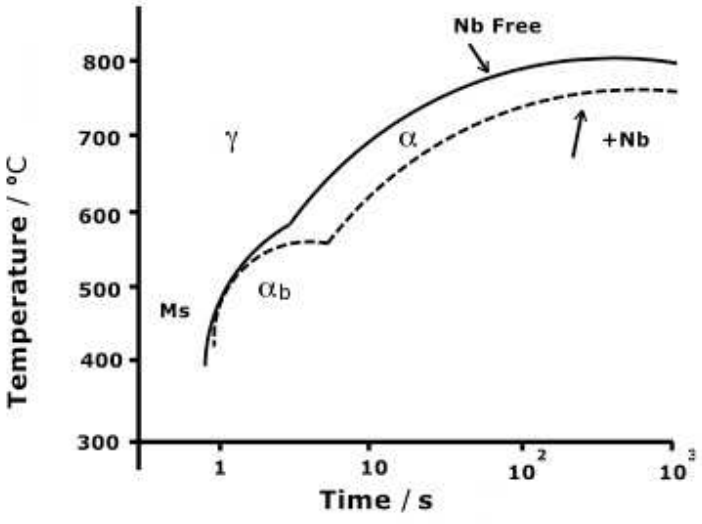

Figure 1: TTT diagram adapted from [5].

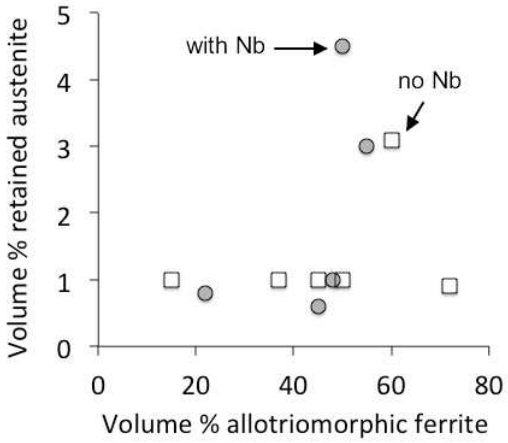

Figure 2: A selection of data on TRIP-assisted steels, one of which contains niobium. The data are for the case where the austenite is in a recrystallised state, and the original work [18] did not comment on any uncertainties in the volume fraction determinations.

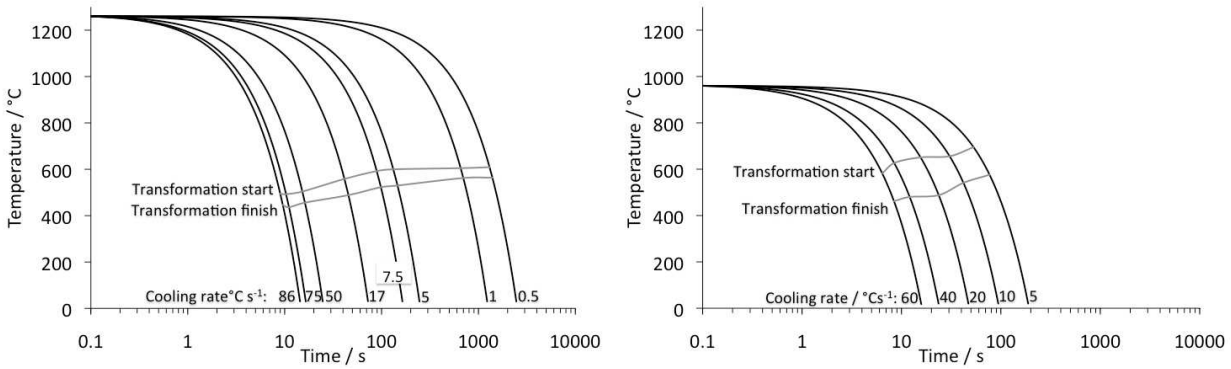

(a) Austenitised at 1260°C for 1 min.

(b) Austenitised at 960°C for 5 min.

Figure 3: Continuous–cooling–transformation (CCT) diagram of the X80 steel. The cooling rate is measured between 800 and 500°C. The transformation start and finish temperatures were determined using the offset method [55] on the continuous cooling dilatometry curves at 1% and 99% transformation respectively.

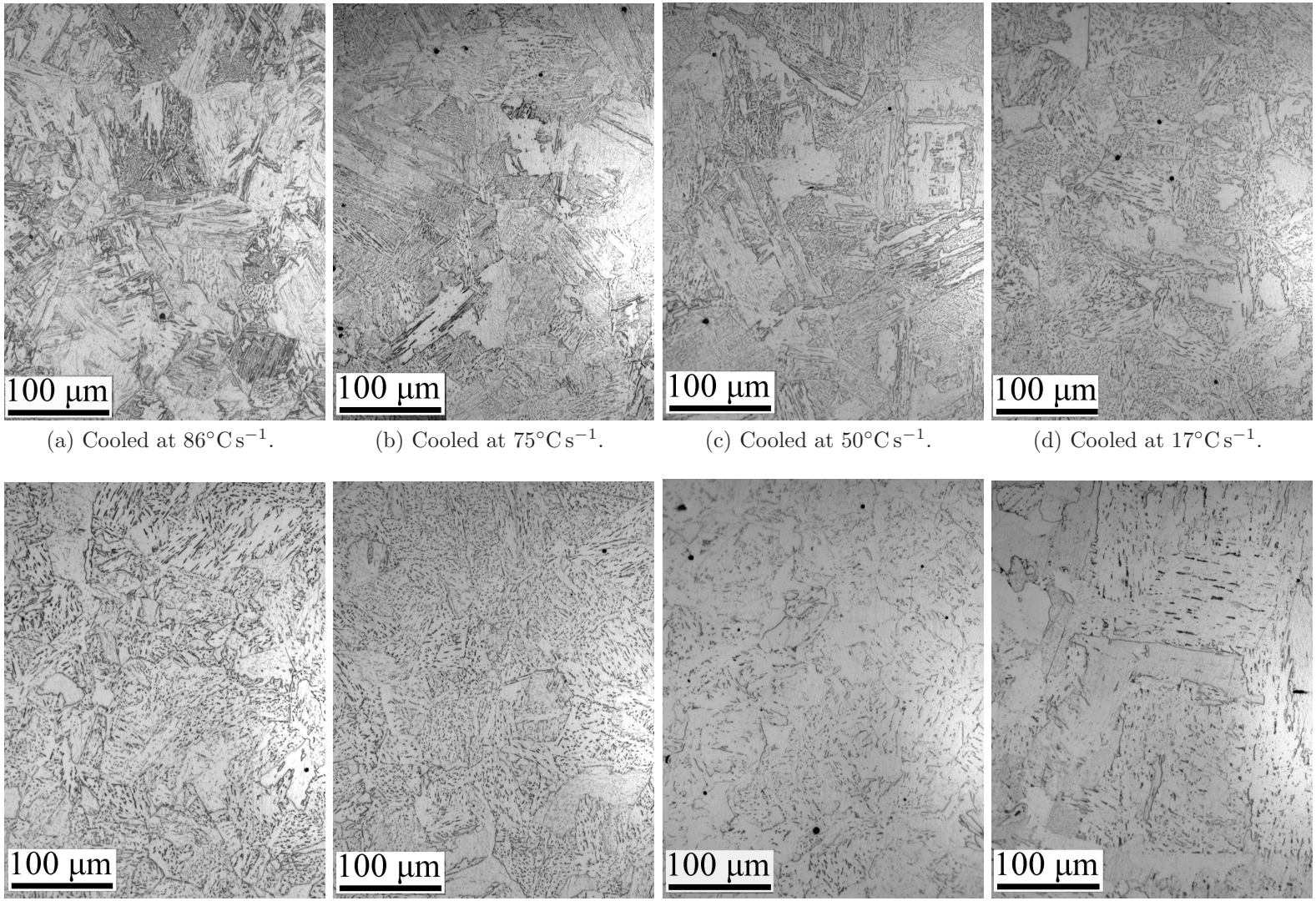

(a) Cooled at 86°C s^{-1}. (b) Cooled at 75°C s^{-1}. (c) Cooled at 50°C s^{-1}. (d) Cooled at 17°C s^{-1}.

(e) Cooled at 7.5°C s^{-1}. (f) Cooled at 5°C s^{-1}. (g) Cooled at 1°C s^{-1}. (h) Cooled at 0.5°C s^{-1}.

Figure 4: Optical micrographs of the continuous cooled samples after austenitisation at 1260°C for 1 min.

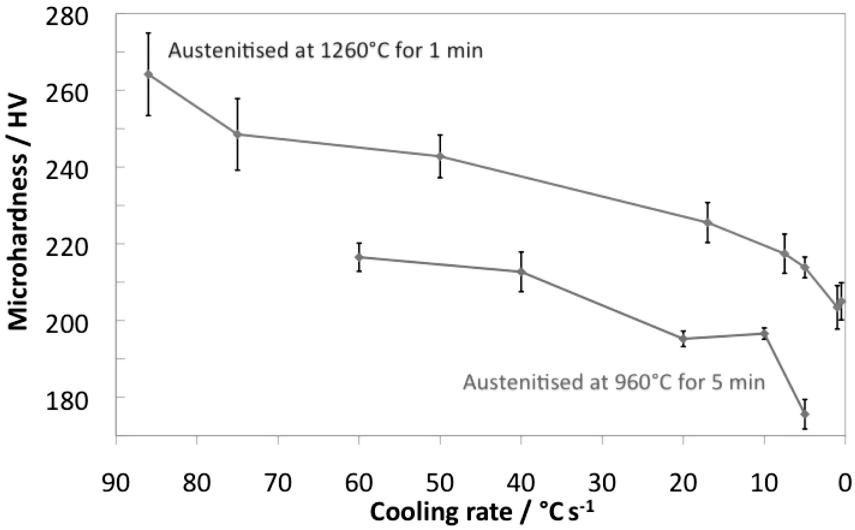

Figure 5: Microhardness values of the continuously cooled samples. The average value and standard deviation of 10 measurements for each sample is plotted.

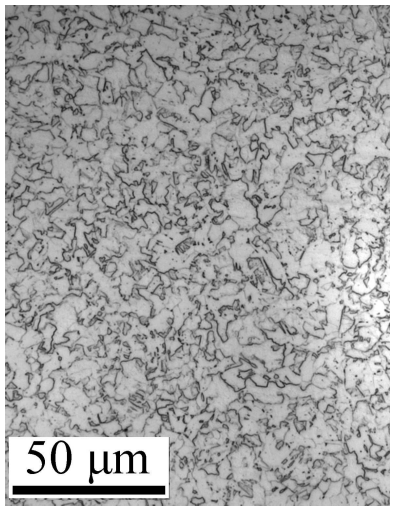

(a) Cooled at $60\,^{\circ}\mathrm{C\,s^{-1}}$.

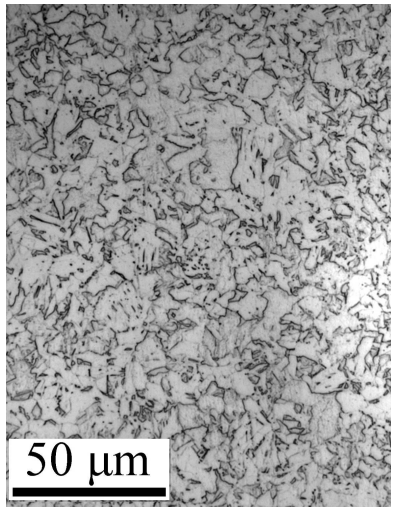

(b) Cooled at $40\,^{\circ}\mathrm{C\,s^{-1}}$.

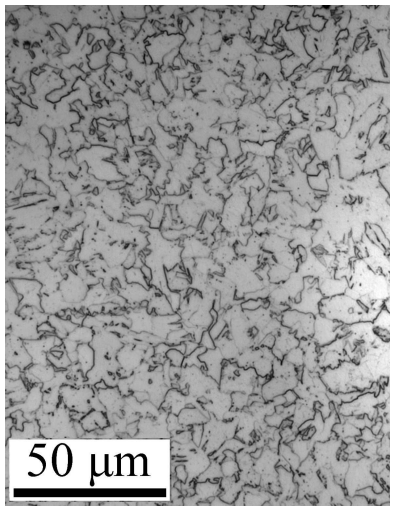

(c) Cooled at $20\,^{\circ}\mathrm{C\,s^{-1}}$.

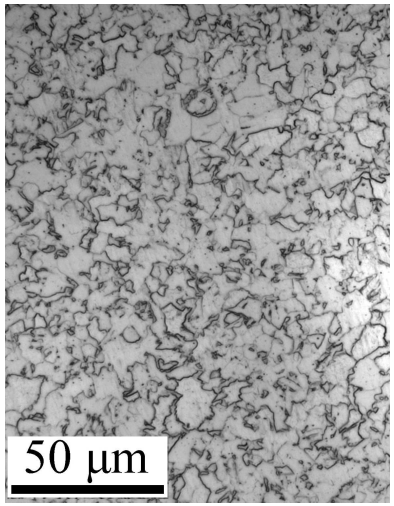

(d) Cooled at $10\,^{\circ}\mathrm{C\,s^{-1}}$.

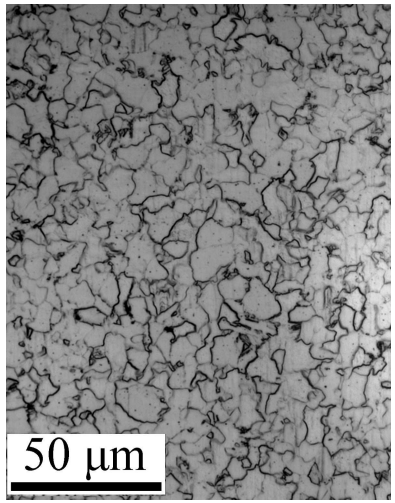

(e) Cooled at $5\,^{\circ}\mathrm{C\,s^{-1}}$.

Figure 6: Optical micrographs of the continuous cooled samples after austenitisation at 960°C for 5 min.

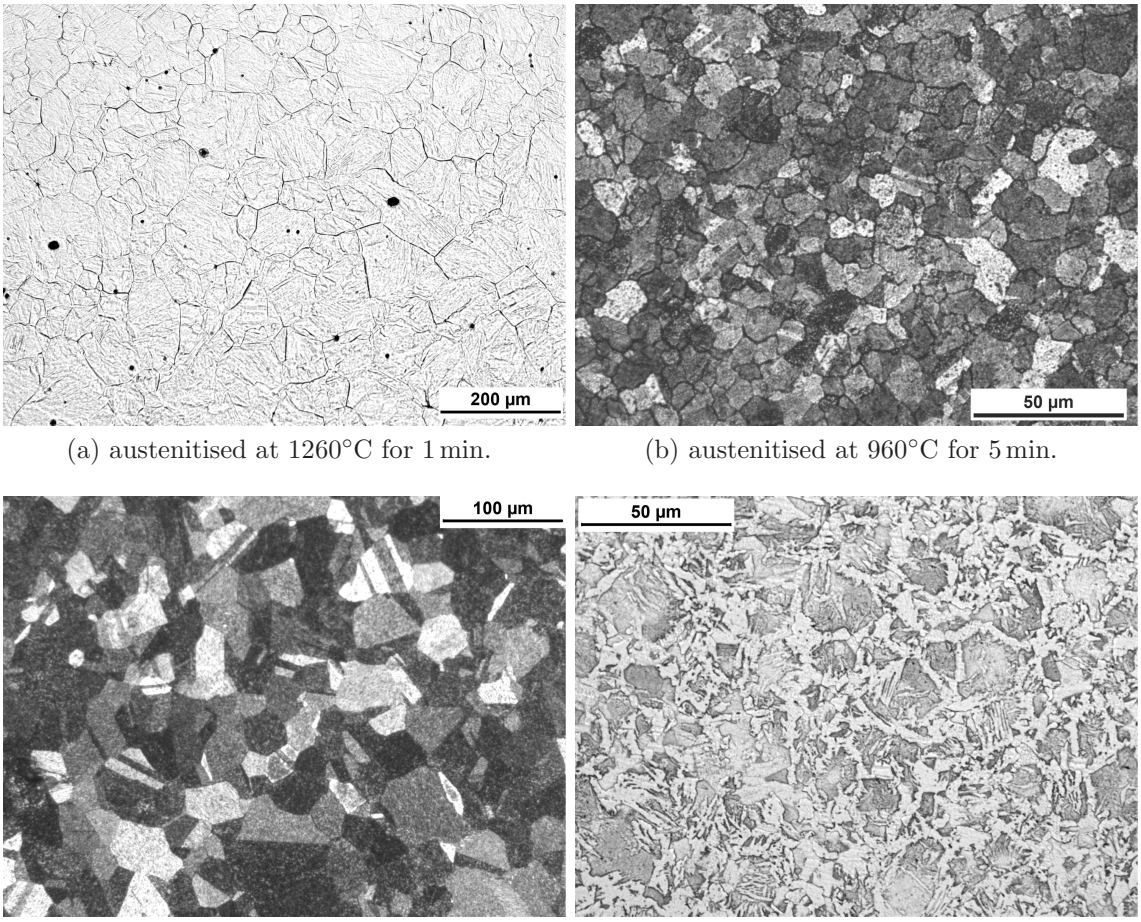

(a) austenitised at 1260°C for 1 min.

(b) austenitised at 960°C for 5 min.

(c) austenitised at 1160°C for 6 s.

(d) austenitised at 960°C for 24 h.

Figure 7: Optical micrographs revealing the prior austenite grains by thermal etching in (a–c) and by etching with 3% nital in (d).

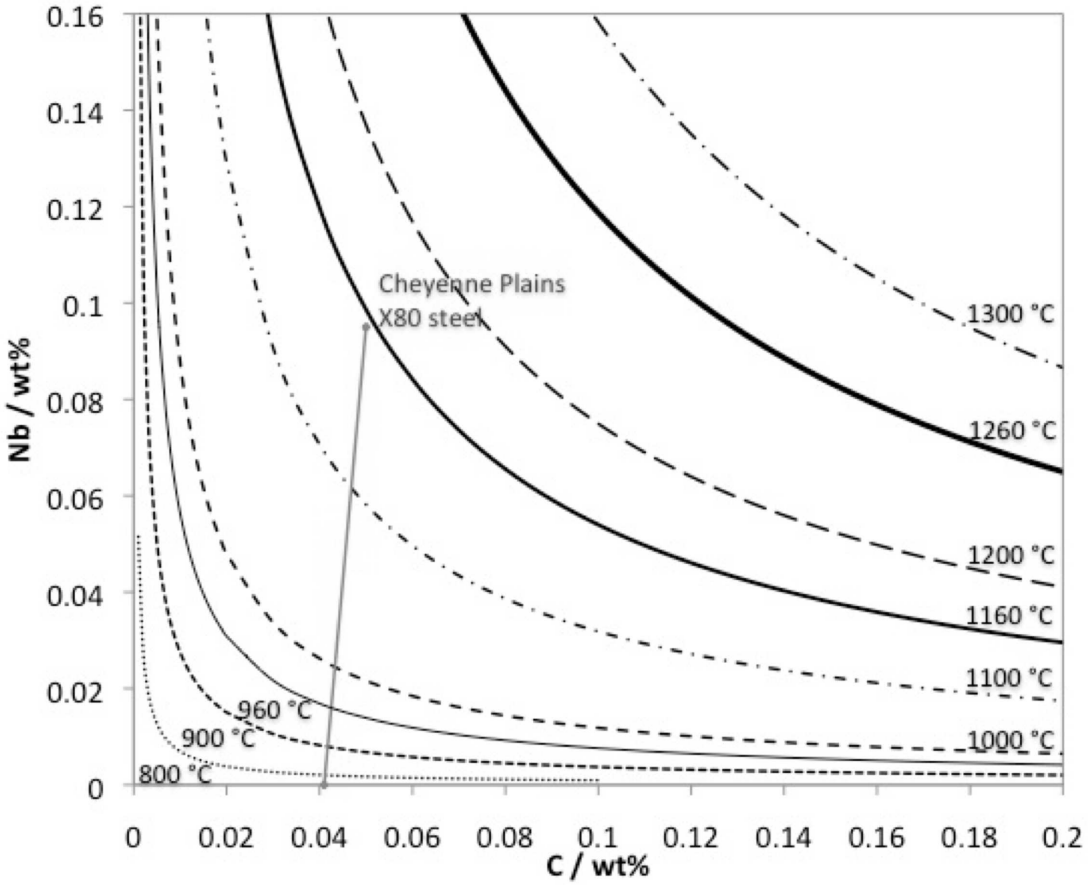

Figure 8: Limits of the mutual solubility of niobium and carbon in austenite, and the stoichiometric ratio line for niobium carbide in the X80 steel.

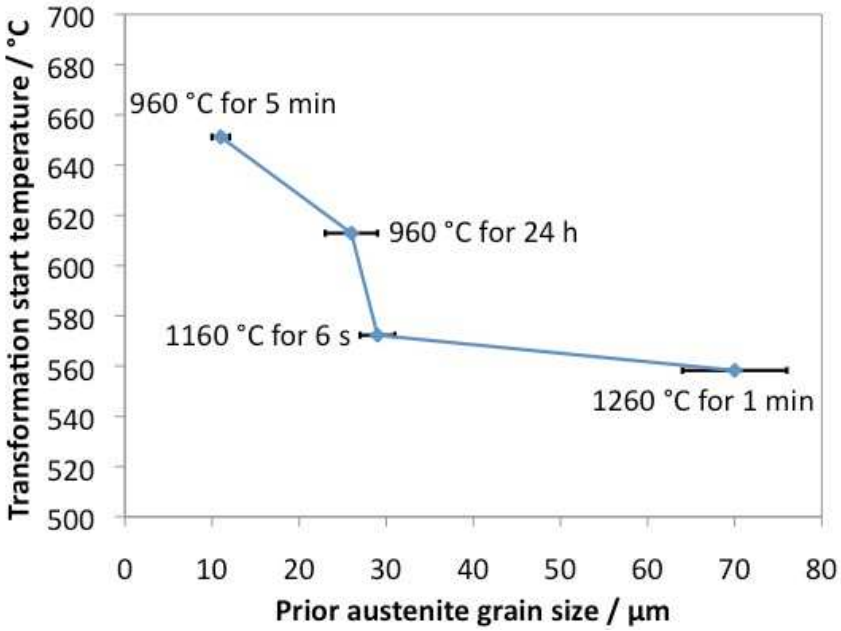

Figure 9: Relation between the transformation-start temperature and the prior austenite grain size at different austenitisation conditions followed by the same cooling rate of $20\,^{\circ}\mathrm{C\,s^{-1}}$.

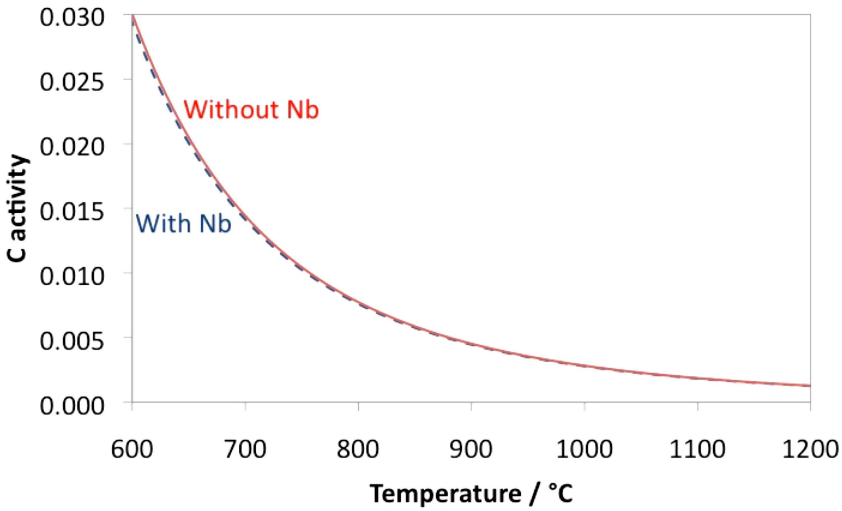

Figure 10: Carbon activity in austenite of the steel studied in this work calculated using MTDATA [56].

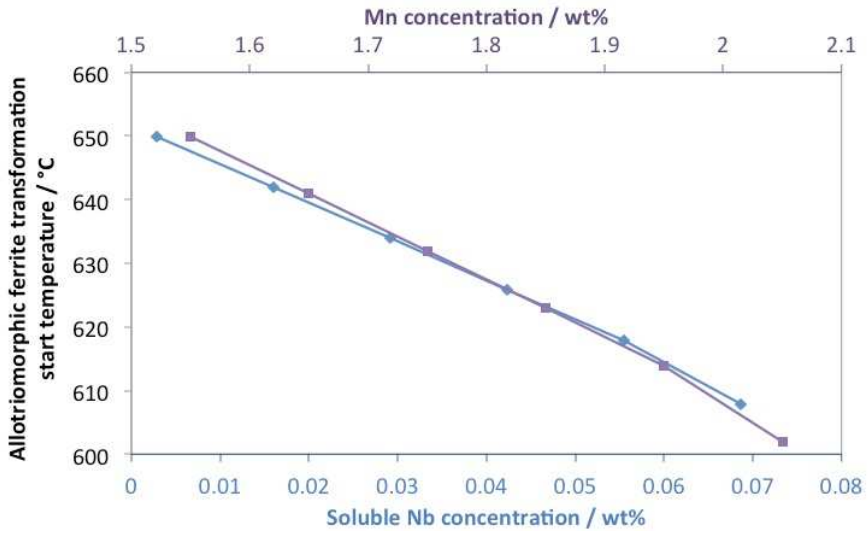

Figure 11: The effects of Nb and Mn on the allotriomorphic ferrite transformation start temperature using kinetic theory [48, 51].